A DYNAMIC NUMERICAL MODEL OF TRANSMEMBRANE VOLTAGE INDUCEMENT AND ELECTROPORATION ON IRREGULARLY SHAPED CELLS

Gorazd Pucihar, Tadej Kotnik, Damijan Miklavčič

University of Ljubljana, Faculty of Electrical Engineering,
1000 Ljubljana, Tržaška 25, Slovenia

gorazd.pucihar@fe.uni-lj.si (Gorazd Pucihar)

Abstract

We recently presented a method for constructing realistic three-dimensional numerical models of irregularly shaped cells from their cross-section fluorescence images. The model enables the calculation of the steady-state value of the induced transmembrane voltage (ITV) on the same cells on which an experiment was carried out. This model was now extended to allow also the calculation of dynamic changes of the ITV. The results of calculations were first verified by comparison to the dynamic analytical solution for the ITV on a spherical cell, and a good agreement was obtained. To model the process of electroporation, the model was modified to allow also the changes of electric conductivity of the cell membrane. The calculations were performed on a model of a spherical and an irregularly shaped cell. In both cases, a time dependent increase of membrane conductivity was observed, but only in the regions of the membrane where ITV exceeded a threshold value. In the regions of elevated membrane conductivity the ITV decreased with time and its spatial distribution was changed, and these changes are in agreement with literature. The regions of increased membrane conductivity, calculated for the model of irregularly shaped cell, corresponded to experimentally observed regions of molecular transport. Both models, the dynamic model of the ITV and the model of electroporation, can be exploited further to study the behavior of more complicated cell systems.

Keywords: finite elements modeling, induced transmembrane voltage, irregularly shaped cells, electroporation

Presenting Author's biography

Gorazd Pucihar was born in Ljubljana, Slovenia in 1976. He received the Ph.D. degree in Electrical Engineering from the University of Ljubljana, Slovenia, and the Ph.D. degree from the University Paul Sabatier, Toulouse III, France.
His research work is focused on experimental investigation and numerical modeling of the process of electroporation. He is currently employed as a Research Associate at the Faculty of Electrical Engineering, University of Ljubljana.

ISBN 978-3-901608-32-2

1 Introduction

When a cell is exposed to a short and sufficiently strong external electric field, a transient increase in membrane permeability occurs - a phenomenon termed electropermeabilization or electroporation. This allows the introduction of ions and small molecules (e.g. drugs, fragments of DNA…), which are impermeant for the intact membrane, to enter the cells [1, 2].

It was shown experimentally that electroporation occurs in those regions of the membrane where the transmembrane voltage induced by the external electric field (ITV) is the highest [3]. In order to obtain an efficient cell electroporation it is therefore important to determine the distribution of the ITV on the cell membrane. The distribution of the ITV can be of interest also in other theoretical and experimental settings besides electroporation, for example, for the activation of voltage-dependent membrane channels.

For cells of simple geometrical shapes, such as spheres and ellipsoids, the analytical solution for ITV can be derived. For example, for a spherical cell with radius R, exposed to a step turn-on of a DC electric field, the analytical solution for the ITV reads [4, 5]:

$$ITV(t) = f_s ER\cos\theta\left(1-\mathrm{e}^{(-t/\tau)}\right), \qquad (1)$$

Here, θ is the angle between the direction of the applied electric field E and the normal from the center of the cell to the point of interest on the cell surface, t denotes the time from the turn-on of the field. The function f_S and the time constant τ are given by:

$$f_S = \frac{3\lambda_o\left(3dr^2\lambda_i + \left(3d^2r - d^3\right)\left(\lambda_m - \lambda_i\right)\right)}{\left(\begin{array}{l} 2r^3\left(\lambda_m + 2\lambda_o\right)\left(\lambda_m + 0.5\,\lambda_i\right) - \\ -2\left(r-d\right)^3\left(\lambda_o - \lambda_m\right)\left(\lambda_i - \lambda_m\right) \end{array}\right)} \qquad (2)$$

$$\tau = \frac{Rc_m}{\dfrac{2\lambda_o\lambda_i}{2\lambda_o + \lambda_i} + \dfrac{R}{d}\lambda_m}, \quad c_m = \varepsilon_m / d\,, \qquad (3)$$

with c_m the membrane capacitance, d the membrane thickness, and λ_i, λ_m, λ_o the conductivities of the cytoplasm, cell membrane, and extracellular medium, respectively. Similar analytical solutions for ITV were also derived for spheroidal cells [6, 7].

However, for realistic cells, which have more complicated shapes, the analytical solution is not attainable and the ITV can only be determined experimentally [3, 8, 9] or numerically [9-12]. We recently developed a method for constructing realistic finite elements models of cells of irregular shapes and clusters of such cells [9, 13]. These models were used to calculate the ITV, but the results were only valid for the steady-state conditions. As such, these models were also not appropriate for modeling the process of electroporation. Here, we present an extension of this steady-state numerical model, which enables the calculation of dynamic changes of ITV on cells of irregular shape. Besides, the model of electroporation is also presented.

2 Materials and Methods

2.1 Construction of a realistic 3D numerical model of a cell

Three-dimensional model of an irregularly shaped cell was constructed from a sequence of microscopic fluorescence images representing cross-sections of a Chinese Hamster Ovary (CHO) cell attached to the cover glass. A detailed description of the model construction can be found in [9]. Briefly, fluorescence images were obtained by staining the cell with a fluorescent dye Di-8-ANEPPS. The images, acquired with a CCD camera (VisiCam 1280, Visitron, Germany) mounted on a fluorescence microscope (AxioVert 200, Zeiss, Germany), were processed to obtain contours of the cell edges. The contours were transformed to solid planes, combined into a 3D object and imported to the COMSOL workspace (COMSOL Inc., Burlington, MA, USA) (Fig. 1).

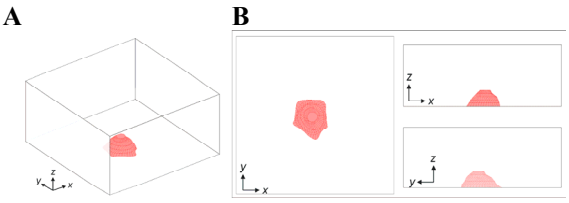

Fig. 1 Numerical model of an attached CHO cell. (A) The three-dimensional geometry of the model of a cell constructed from four parallel horizontal cross-sections. The model of a cell is placed at the bottom of the cube to mimic the cell attached to coverglass. The dimensions of the box were 79×79×38 µm. The grey-shaded faces are the electrodes, one set to 7.9 V and the other to the ground (electric field 1000 V/cm). (B) Different side views of the model.

2.2 Settings of the model and calculations of the induced transmembrane voltage

The calculations were performed in COMSOL using the *electric currents, transient analysis* application mode. The conductivity of the cell interior was set to 0.3 S/m and that of the cell exterior to 0.14 S/m [5, 9]. The opposite vertical faces of the block were modeled as electrodes, which was done by assigning a fixed electric potential to each of these faces. One electrode was set to 7.9 V and the other to the ground to obtain the electric field of 1000 V/cm, which was the field used in the experiments (see below). The remaining faces of the block were modeled as insulating.

After the mesh was generated, the electric potential φ was computed using finite elements method with COMSOL 3.1 (direct SPOOLES solver was used), by

solving the equation:

$$-\nabla(\lambda\nabla\varphi)-\varepsilon_0\varepsilon_r\nabla\left(\frac{\partial}{\partial t}(\nabla\varphi)\right)=0\,. \qquad (4)$$

In the above equation, ε_0 is dielectric permittivity of the vacuum, ε_r is relative dielectric permittivity, and λ is conductivity. The ITV was then calculated as the difference between electric potentials on both sides of the membrane: $ITV(t) = \varphi_i(t) - \varphi_o(t)$ and plotted as a function of the arc length.

2.3 Modeling the cell membrane

Direct incorporation of a realistic cell membrane into the model is difficult. If the events inside the membrane are not of interest, the membrane can be replaced by a surface to which a boundary condition is assigned [9]:

$$J(t)=\frac{\lambda_m(\varphi_o-\varphi_i)}{d}+\frac{\varepsilon_m}{d}\frac{\partial(\varphi_o-\varphi_i)}{\partial t}\,. \qquad (5)$$

Here, J is the current density, λ_m is the membrane conductivity, d is the membrane thickness, ε_m is the dielectric permittivity of the membrane and φ_o, φ_i are the electric potentials at the outer and inner surface of the membrane, respectively. In a model constructed in this way, the mesh of finite elements is generated without difficulty, as very small elements corresponding to the membrane are avoided (Fig. 2) [9].

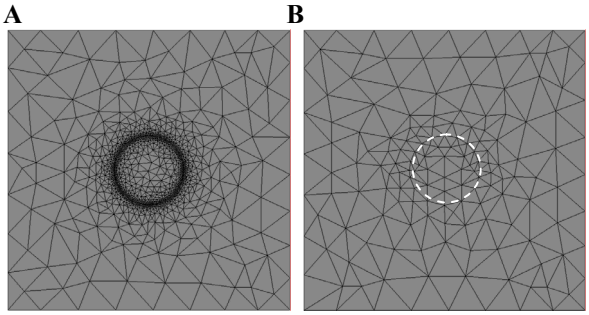

Fig. 2 Comparison of mesh of finite elements for a model of a spherical cell with radius 10 μm. A cross-section through the center of the cell is shown. (A) Membrane with thickness of 0.3 μm was incorporated in the model, which is still about 70 times thicker than the real membrane. Number of mesh elements was 199000. (B) Membrane was modeled as a boundary condition. Number of mesh elements was 3746. More details can be found in [9].

2.4 Model of electroporation

It was shown experimentally that during electroporation, the membrane conductivity in the electroporated regions increases by several orders of magnitude [3, 14]. Besides, electroporation occurs predominantly in the regions of the membrane where the absolute value of ITV exceeds some threshold value [3]. Therefore, we modeled the course of electroporation by changing the conductivity of the membrane (λ_m) in the regions of the membrane where ITV exceeded a threshold value (set at 450 mV – unpublished data). Besides ITV, λ_m depends also on time and both functional dependencies can be arbitrarily chosen. In our case, the dependence of λ_m on ITV was approximated with a sigmoidal function, while the time dependence of λ_m was approximated with an exponential rise to maximum:

$$\lambda_m(ITV,t)=\lambda_0+\left(1-\mathrm{e}^{(-t/\tau)}\right)\cdot \cdot\left[\lambda_{EP}/\left(1+\mathrm{e}^{(-(ITV-ITV_C)/b)}\right)\right] \qquad (6)$$

Here, λ_0 is the conductivity of the intact membrane (3×10^{-7} S/m [5]), τ is the arbitrarily chosen time constant of the λ_m increase (5 μs), λ_{EP} is the conductivity of the electroporated membrane (7×10^{-4} S/m), $ITVc$ is the critical ITV where electroporation occurs (450 mV) and b is the parameter determining the slope of the sigmoidal increase of λ_m with ITV (0.03). The changes in λ_m during the field exposure were modeled as irreversible, so that λ_m either increased or remained constant. We should note that the actual functional dependence of λ_m on ITV and time is not known precisely. The selected functions were therefore chosen as they are simple enough not to cause numerical errors in the Comsol. They can be replaced with more appropriate functions if experimental data are available or if the exact analytical expression is derived.

2.5 Monitoring the course of electroporation

Chinese hamster ovary cells (CHO) were grown on cover glasses in culture medium (F-12, Sigma, Saint Louis, USA). When cells attached to the glass (approx 12 hours after plating) the medium was replaced by a pulsing buffer [9], which contained 100 μM of membrane-impermeant fluorescent dye Propidium Iodide (PI, Sigma, Saint Louis, USA). Cells were then exposed to a 400 V, 200 μs electroporating pulse delivered to the parallel electrodes with a 4 mm distance between them (1000 V/cm). The fluorescence of the dye increased considerably after entering the electroporated cell, which was detected with an imaging system described in Section 2.1.

3 Results and discussion

3.1 Time course of transmembrane voltage induced on a spherical cell

The model was first validated by a comparison of the ITV calculated on a model of a spherical cell, with the analytical solution. The spatial distribution of the electric potential in the model at different times after the onset of the external electric field (1000 V/cm) is shown in Fig. 3A. From these results the ITV was determined as the difference between potentials on both sides of the membrane ($ITV(t) = \varphi_i(t) - \varphi_o(t)$; Fig. 3B). The calculations show that after a step change of the electric field, the ITV gradually forms across the

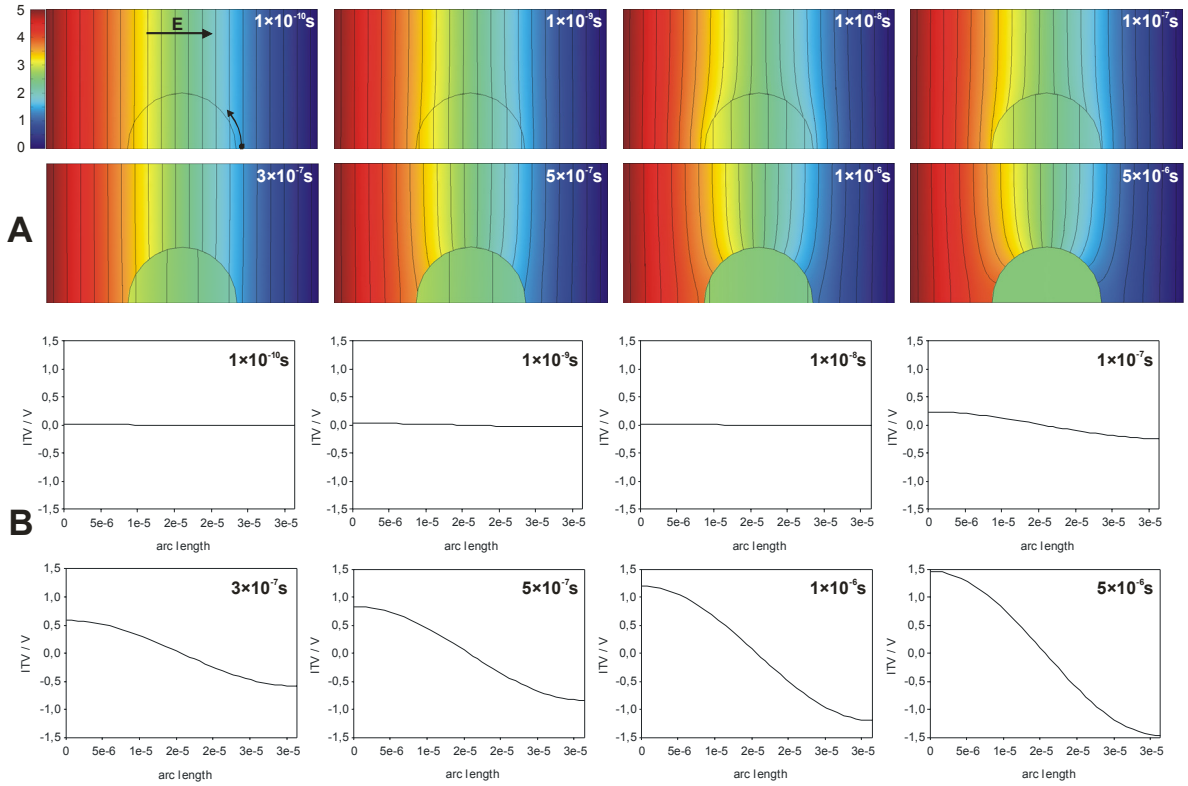

Fig. 3 (A) The calculated distribution of the electric potential around and inside a spherical cell in the x-y plane crossing the center of the cell. The black curves are the equipotentials, the arrow marks the path along which the potential was measured. The scale is in volts. (B) Corresponding time courses of ITV. R = 10 µm, d = 5 nm, λ_o = 0.14 S/m, λ_i = 0.3 S/m, $\lambda_m = 3\times10^{-7}$ S/m, $\varepsilon_m = 4.4\times10^{-11}$ As/Vm, $\varepsilon_o = \varepsilon_i = 7.1\times10^{-10}$ As/Vm (values taken from [5, 9], E = 1000 V/cm.

cell membrane and reaches its steady state value after a few microseconds. The calculated ITV was then compared to the analytically derived (Eq. 1), and a good agreement was obtained (Fig. 4).

3.2 Modeling electroporation

To model the course of electroporation, the model was modified in order to allow the changes in the electric conductivity of the cell membrane. Namely, it was shown experimentally that electroporation is accompanied by an increase in the membrane conductivity, and this increase was observed only in the regions of the membrane where the absolute value of ITV exceeded a threshold value (in our case 450 mV) [3]. We first modeled electroporation for the case of a spherical cell exposed to 1000 V/cm. Changes in membrane conductivity, which indicate electroporation, are shown in Fig. 5A and confirm the experimental observations, namely, the membrane conductivity increases with time but only in the regions where ITV exceeds a threshold value. The spatial distribution of ITV is depicted in Fig. 5B (black curves) and shows a time-dependent increase of ITV until the critical value of 450 mV is exceeded (at 3×10^{-7} s), when electroporation occurs. Because at this point, the membrane conductivity starts to rapidly increase (Fig. 5B, red curves), the ITV in the electroporated regions consequently decreases, while its spatial distribution deforms with respect to the cosine form observed on the intact membrane. The calculated time course of ITV during electroporation, which is shown in Fig. 5B (black curves) is similar to the ITV, which was measured by Hibino and co-workers by using a fast imaging system and a potentiometric fluorescent dye [3].

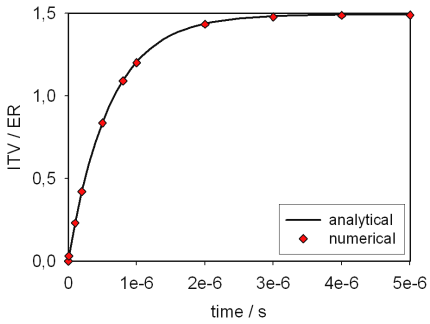

Fig. 4 Time course of transmembrane voltage inducement. Line presents the analytically calculated ITV (Eq. 1, cos θ = 0), while the symbols are numerically calculated ITV (see Fig. 3).

Next, a realistic model of an irregularly shaped cell was constructed (Fig. 5C and D) and similar calculations were performed. The time course and spatial distribution of electroporation and ITV are slightly different from those observed for a spherical cell, which is a consequence of different shape and

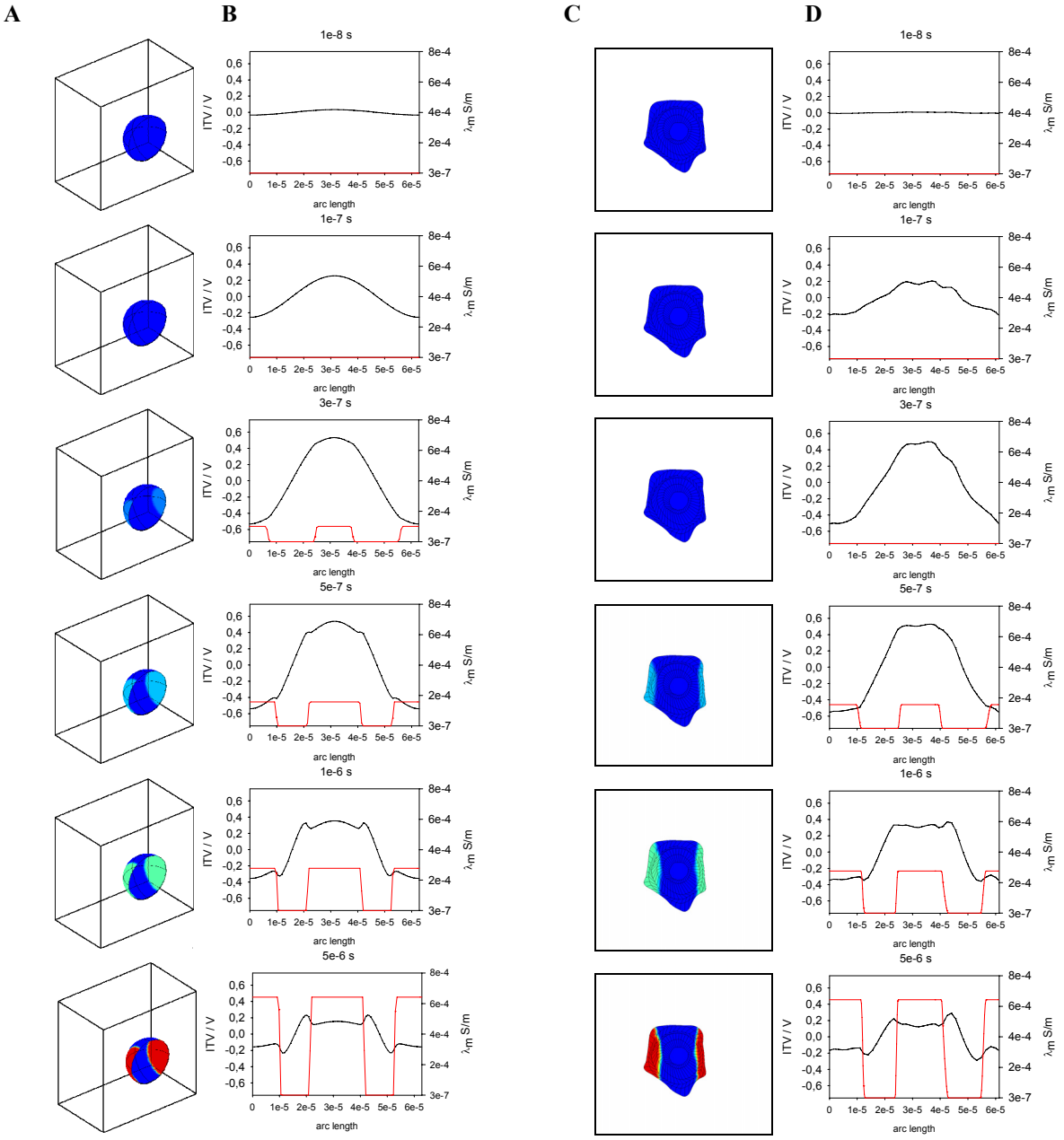

Fig. 5. *Left column: Spherical cell.* (A) A 3D presentation of the changes in membrane conductivity (λ_m). The arrow marks the path along which the ITV and λ_m were sampled. The scale is in S/m. (B) ITV (black) and λ_m (red) as a function of arc length. ITV_C = 450 mV.
Right column: Attached cell. (A) Changes in membrane conductivity for ITV_C = 450 mV shown for x-y plane. The arrow marks the path along which the ITV and λ_m were sampled. The scale is in S/m. (B) ITV (black) and λ_m (red) as a function of arc length. Model settings are the same as in Fig. 4.

orientation of both models in the electric field. The undulations in the spatial distribution of ITV, such as at time 1×10^{-7} s (Fig. 5D) for example, are the effect of the shape of the cell and do not reflect electroporation. These undulations show, however, that in applications, which require a detailed determination of the course of ITV on a cell membrane, realistic numerical models of cells, such as the one presented here, are necessary.

3.3 Experimental monitoring of electroporation

Irregularly shaped cell from which the model in Fig. 5C was constructed was then used in an experiment. This is the advantage of the method of model construction [9, 13], because it allows a direct comparison of experiments with calculations. The cell in our case was exposed to a high voltage electroporation pulse (1000 V/cm) and the transport of molecules through electroporated cell membrane was monitored. Figure 6 is a time sequence of fluorescence

images showing the transport of fluorescent molecules through electroporated regions of the membrane. The regions where the transport of molecules occurred correspond to the calculated regions of increased membrane conductivity (cf. Figs. 5C, and 6A). We should note, however, that the time scale is different. Namely, changes of membrane conductivity occur within microseconds after the onset of the electric pulse, while the transport, also in part limited by the sensitivity of the imaging camera, can not be detected earlier then several miliseconds after the pulse. Whether molecular transport starts simultaneously with the increase of membrane conductivity remains to be elucidated.

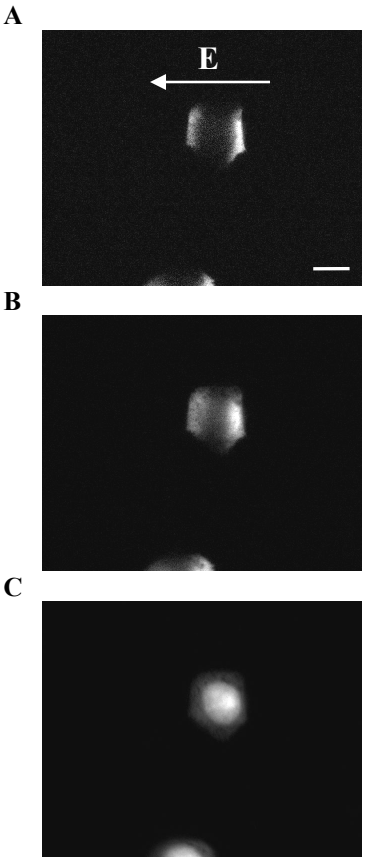

Fig. 6. Monitoring cell electroporation (A) 100 ms, (B) 1500 ms, and (C) 3 min after pulse delivery. The cell was exposed to a single 400 V (1000 V/cm) rectangular pulse (200 μs). To visualize the electroporated regions Propidium Iodide was added to suspension before the pulse was applied. The bar in Fig. A corresponds to 10 μm.

4 Conclusions

A dynamic model of transmembrane voltage inducement and electroporation was presented, which is an extension of the recently published steady-state model. A good agreement was obtained between the calculated time course of ITV and the analytical solution for a spherical cell, confirming the validity of the model. Electroporation was modeled by changing the electric conductivity of the membrane. The calculations performed on spherical and irregularly shaped cell showed a time dependent increase in membrane conductivity, but only in the regions of the membrane where ITV exceeded a threshold value. Consequently, the spatial distribution of ITV in these regions deformed and decreased with time, as reported also in literature. The regions of increased membrane conductivity, calculated for an irregularly shaped cell, corresponded to the experimentally observed regions of molecular transport on the same cell. Whether the transport starts simultaneously with the change of membrane conductivity remains to be elucidated. Both models presented here - the dynamic model of the ITV and the model of electroporation - can be exploited further to study the behavior of more complicated cell systems, such as several irregularly shaped cells in contact, in response to electric field exposure.

5 Acknowledgements

This work was supported by the Slovenian Research Agency.

6 References

[1] T. Y. Tsong. Electroporation of cell membranes. *Biophys J,* 60:297-306, 1991.

[2] J. Teissié, N. Eynard, B. Gabriel, and M. P. Rols. Electropermeabilization of cell membranes. *Adv Drug Deliver Rev,* 35:3-19, 1999.

[3] M. Hibino, H. Itoh, and K. Jr. Kinosita. Time courses of cell electroporation as revealed by submicrosecond imaging of transmembrane potential. *Biophys J*, 64:1789-1800, 1993.

[4] H. Pauly, and H. P. Schwan. Uber die Impedanz einer Suspension von kugelformigen Teilchen mit einer Schale, Z. Naturforsch., B: *Anorg Chem, Org Chem,* 14:125–131, 1959.

[5] T. Kotnik, D. Miklavčič, and T. Slivnik. Time course of transmembrane voltage induced by time-varying electric fields – a method for theoretical analysis and its application. *Bioelectrochem Bioenerg*, 45:3-16, 1998.

[6] T. Kotnik, and D. Miklavčič. Analytical description of transmembrane voltage induced by electric fields on spheroidal cells. *Biophys J,* 79: 670-679, 2000.

[7] J. Gimsa, and D. Wachner. Analytical description of the transmembrane voltage induced on arbitrarily oriented ellipsoidal and cylindrical cells. *Biophys J,* 81:1888–1896, 2001.

[8] D. Gross, L. M. Loew, and W. Webb. Optical imaging of cell membrane potential changes induced by applied electric fields. *Biophys J*, 50:339-348, 1986.

[9] G. Pucihar, T. Kotnik, B. Valič, and D. Miklavčič. Numerical modeling of induced transmembrane voltage induced on irregularly shaped cells. *Ann Biomed Eng*, 34:642-652, 2006.

[10] C. E. Miller, and C. S. Henriquez. Three-dimensional finite element solution for biopotentials: erythrocyte in an applied field. et al. *IEEE T Bio-Med Eng*, 35:712-718, 1988.

[11] E. C. Fear, and M. A. Stuchly. Modeling assemblies of biological cells exposed to electric fields. *IEEE Trans Biomed Eng,* 45:1259–1271, 1998.

[12] T. R. Gowrishankar, and J. C. Weaver. An approach to electrical modeling of single and multiple cells. *Proc Natl Acad Sci USA,* 100:3203-3208, 2003.

[13] G. Pucihar, T. Kotnik, and D. Miklavčič. An experimental and numerical study of the induced transmembrane voltage and electroporation on clusters of irregularly shaped cells. In T. Jarm, P. Kramar, A. Županič, editors, *11th Mediterranean Conference on Medical and Biological Engineering and Computing*, IFMBE Proceedings, Vol. 16, page 639-642, Ljubljana, 26-30 June 2007.

[14] K. Kinosita, and T. Y. Tsong. Voltage-Induced conductance in human erythrocyte membranes. *Biochim Biophys Acta*, 554:479-497, 1979.

ISBN 978-3-901608-32-2